

Time-Series of Sentinel-1 Interferometric Coherence and Backscatter for Crop-Type Mapping

Alejandro Mestre-Quereda, *Member, IEEE*, Juan M. Lopez-Sanchez [✉], *Senior Member, IEEE*,
Fernando Vicente-Guijalba, *Member, IEEE*, Alexander W. Jacob [✉], *Member, IEEE*, and Marcus E. Engdahl

Abstract—The potential use of the interferometric coherence measured with Sentinel-1 satellites as input feature for crop classification is explored in this study. A one-year time-series of Sentinel-1 images acquired over an agricultural area in Spain, in which 17 crop species are present, is exploited for this purpose. Different options regarding temporal baselines, polarization, and combination with radiometric data (backscattering coefficient) are analyzed. Results show that both radiometric and interferometric features provide notable classification accuracy when used individually (overall accuracy lies between 70% and 80%). It is found that the shortest temporal baseline coherences (6 days) and the use of all available intensity images perform best, hence proving the advantage of the 6-day revisit time provided by the Sentinel-1 constellation with respect to longer revisit times. It is also shown that dual-pol data always provide better classification results than single-pol ones. More importantly, when both coherence and backscattering coefficient are jointly used, a significant increase in accuracy is obtained (greater than 7% in overall accuracies). Individual accuracies of all crop types are increased, and an overall accuracy above 86% is reached. This proves that both features provide complementary information, and that the combination of interferometric and radiometric radar data constitutes a solid information source for this application.

Index Terms—Agriculture, crop classification, interferometry, synthetic aperture radar.

I. INTRODUCTION

THEMATIC maps of agricultural crop types constitute a valuable product of satellite remote sensing. This kind of maps provides both updated and reliable information to agencies and producers, either at local or national level. They also enable us to monitor farming activities, check crop rotations, help

future decision-making, and other actions directly related to socioeconomic aspects of this primary sector.

To date, most crop classification approaches employ optical or multispectral data as input features, due to their well-known sensitivity to crop biophysical properties. However, the number and/or the quality of these images may be insufficient over some geographical regions and/or at important dates due to the presence of clouds, haze, etc. Alternatively, approaches using images acquired by synthetic aperture radar (SAR) sensors, which are able to gather data independently from weather conditions and sun illumination, can contribute to overcome these limitations. The use of SAR images for crop-type mapping has gained attraction in the last years due to the availability of consistent time series of SAR data provided by the last generation of radar satellites. In this context, the free access to Sentinel-1 images acquired over Europe every 6 days constitutes a key motivation to exploit this information source for crop classification.

Conventional SAR-based mapping methods employ radiometric information, that is, time-series of backscatter coefficients (intensities) and/or indices derived from them (such as the ratios) are used as input to classification algorithms. In this regard, it is worth mentioning that time-series of Sentinel-1 radiometric data have proven effective and valuable in this context, as shown with some previous works concerning crop-type mapping in different areas [1]–[4].

Another way of exploiting SAR data consists of generating time-series of interferometric images, which come from the combination of two SAR images acquired at different dates. Repeat-pass SAR interferometry (InSAR) [5] is useful to detect changes in the scene between the two acquisitions since they cause a decrease in interferometric coherence. This loss of coherence is usually denoted as temporal decorrelation. In fact, the primary cause of coherence loss over agricultural crops is temporal decorrelation, since the rest of decorrelation sources, including volume decorrelation, are close to 1. In a broader context, repeat-pass interferometry was tested in the past for land cover mapping by using time-series of ERS tandem data [6], [7], with 1-day revisit time, and more recently with Sentinel-1 constellation data [8], [9], with 6-day revisit time. It is important to clarify that this work is focused on crop classification, which is an application domain different from the generic land cover mapping addressed in [8], [9]. Repeat-pass interferometry was also used in agriculture studies in the past [10] using ERS data. Very recently, both single-pass and repeat-pass interferometric coherence measured at X-band by the TanDEM-X mission

Manuscript received April 21, 2020; revised June 19, 2020; accepted July 3, 2020. Date of publication July 9, 2020; date of current version July 24, 2020. This work was supported in part by the European Space Agency via the ESA SEOM Program ITT under Grant AO/1-8306/15/I-NB “SEOM-S14SCI Land,” in part by the Spanish Ministry of Science, Innovation and Universities, the State Agency of Research (AEI), and in part by the European Funds for Regional Development (EFRD) under Project TEC2017-85244-C2-1-P. (Corresponding author: Juan M. Lopez-Sanchez.)

Alejandro Mestre-Quereda and Juan M. Lopez-Sanchez are with the Signals, Systems and Telecommunications Group, IUII, the University of Alicante, 03080 Alicante, Spain (e-mail: alejandro.mestre@ua.es; juanma.lopez@ua.es).

Fernando Vicente-Guijalba is with the Dares Technology, 08860 Barcelona, Spain (e-mail: fvicente@dares.tech).

Alexander W. Jacob is with the Institute for Earth Observation, Eurac Research, 39100 Bolzano, Italy (e-mail: alexander.jacob@eurac.edu).

Marcus E. Engdahl is with the European Space Research Institute, European Space Agency, 00044 Frascati, Italy (e-mail: marcus.engdahl@esa.int).

Digital Object Identifier 10.1109/JSTARS.2020.3008096

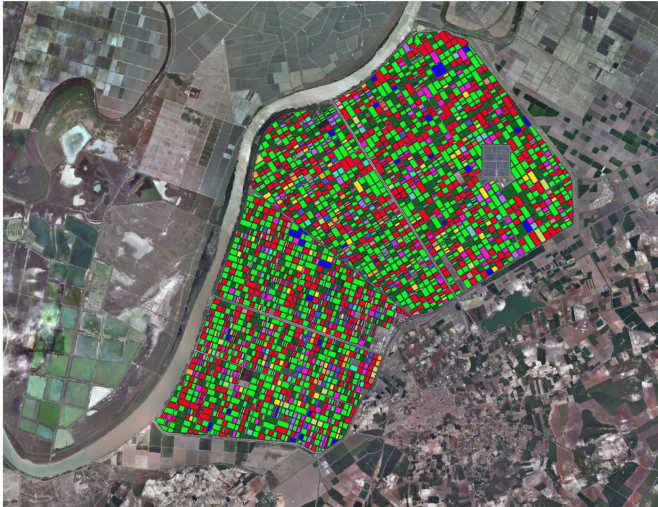


Fig. 1. Map of the reference data over an orthophoto of the test site. Color coding is defined in Fig. 3.

(i.e., with 11-day revisit time) have been tested for crop-type mapping [11].

For the specific application of crop-type mapping, temporal decorrelation is present in areas with vegetation due to wind (and other weather events) and also due to changes in the scene induced by the vegetation itself (such as crop growth during vegetative phases). Contrarily, bare surfaces usually keep a high coherence over longer periods. Consequently, the absence of vegetation, especially at the beginning of the season and after harvest, is expected to be detected by repeat-pass interferometry over agricultural areas. The presence or absence of vegetation would provide information related to the crop calendar, which normally depends on the crop type, hence being useful for crop-type mapping.

In this work, we analyze the use of Sentinel-1 interferometric coherence for crop-type mapping. The goal is to prove that InSAR is also sensitive to the temporal evolution of crops and, hence, that it can be used as an alternative or a complement to traditional SAR-based or intensity-based classifications. The same classification strategy is followed in all tests, and we perform a deep analysis of the influence of the temporal separation between the acquisitions (also known as temporal baseline), the complementarity with respect to the radiometric data, and the effect of polarization, since Sentinel-1, by default, provides images in dual-pol mode (VV and VH polarimetric channels).

II. MATERIAL AND METHODS

A. Reference Data

The test site is located in Sevilla (Andalucía, Spain), centered at 37N, 6.1W. It consists of an agricultural area, named BXII Sector, with a wide variety of crop species cultivated during 2017. As shown in Fig. 1, the dominant crops are cotton, tomato, and sugar beet, followed by corn, sunflower, and carrot. The reference data come from the official land-parcel identification system.

B. Sentinel-1 Data

All available single-look complex (SLC) images of year 2017 (60 images in total) acquired in orbit 154 (incidence angle around 38.7°) by the two-satellite constellation Sentinel-1 A/B in interferometric wide swath mode over the test area have been considered.

C. Interferometric Coherence and Multitemporal Coherence Matrix

The interferometric coherence constitutes an essential product in InSAR [5], since it yields the normalized complex correlation between two SAR images and provides a measurement of the quality of the interferometric phase. Its expression is

$$\hat{\gamma} = \frac{E\{S_1 S_2^*\}}{\sqrt{E\{S_1 S_1^*\} \cdot E\{S_2 S_2^*\}}} \quad (1)$$

where $E\{\cdot\}$ is the expectation operator, and S_1 and S_2 are two complex and coregistered SAR images. For practical purposes, and under the assumption that signals S_1 and S_2 have an ergodic behavior, the expectation operator is substituted by a spatial average of an ensemble of pixels inside a window [12]. (1) therefore becomes

$$\gamma = \frac{\frac{1}{L} \sum_{l=1}^L S_1 S_2^*}{\sqrt{\frac{1}{L} \left(\sum_{l=1}^L S_1 S_1^* \right) \cdot \frac{1}{L} \left(\sum_{l=1}^L S_2 S_2^* \right)}} \quad (L > 1) \quad (2)$$

where L is the number of samples in the window. The process of averaging a certain number of pixels is commonly referred as multilook. The magnitude of γ in (2) ranges between 0 and 1, i.e., $|\gamma| \in [0, 1]$. Low values of $|\gamma|$ are found wherever images S_1 and S_2 are decorrelated, whereas high coherences correspond to areas of the scene in which there exists correlation between the images.

This concept can be extended to time-series, namely, series of images spanning a certain period of time. In this regard, if a given dataset is composed by N SAR images, $S_1 \dots S_N$, we can build an $N \times N$ Hermitian, positive semi-definite temporal covariance matrix \hat{C} as

$$\hat{C} = \begin{bmatrix} E\{|S_1|^2\} & E\{S_1 S_2^*\} & E\{S_1 S_3^*\} & \dots & E\{S_1 S_N^*\} \\ E\{S_2 S_1^*\} & E\{|S_2|^2\} & E\{S_2 S_3^*\} & \dots & E\{S_2 S_N^*\} \\ \vdots & \vdots & \vdots & \ddots & \vdots \\ E\{S_N S_1^*\} & E\{S_N S_2^*\} & E\{S_N S_3^*\} & \dots & E\{|S_N|^2\} \end{bmatrix} \quad (3)$$

where the mathematical expectation is substituted in practice by a spatial average (multilook). Note that the covariance matrix \hat{C} contains the evolution of the radiometric information (that is, the series of backscattering coefficient) in its main diagonal, and all possible interferometric combinations of the dataset in its off-diagonal entries.

From (2) and (3), we can easily derive the expression of the temporal coherence matrix $\hat{\Gamma}$, which is a normalized version of

the previous covariance matrix \hat{C}

$$\hat{\Gamma} = \begin{bmatrix} 1 & \gamma_{12} & \gamma_{13} & \dots & \gamma_{1N} \\ \gamma_{21} & 1 & \gamma_{23} & \dots & \gamma_{2N} \\ \vdots & \vdots & \vdots & \ddots & \vdots \\ \gamma_{N1} & \gamma_{N2} & \gamma_{N3} & \dots & 1 \end{bmatrix}. \quad (4)$$

Therefore, $\hat{\Gamma}$ contains the normalized complex correlation (coherence) between all possible combinations of images of the dataset. The absolute value of any element of $\hat{\Gamma}$ directly yields the coherence of that element in the dataset. The coherence matrix is symmetric (i.e., $|\gamma_{ij}| = |\gamma_{ji}|$), so that the upper (or lower) triangular matrix provides the useful coherence data to be used as input features to a classification algorithm. It is therefore easily verified that if a given dataset contains N SAR images, the number of image pairs (and coherence values) is $N \cdot (N - 1)/2$.

If the input set of images is ordered chronologically, it is deduced that elements which are closer to the main diagonal of $\hat{\Gamma}$ matrix show shorter temporal baselines. In this regard, the superdiagonal entries of $\hat{\Gamma}$ (elements located immediately above the main diagonal) correspond to the *shortest baseline* interferometric combinations.

D. Preprocessing of Sentinel-1 Data

The preprocessing steps carried out with the input data are as follows.

- 1) Coregistration of all SLC images to a common master, using precise orbital information and an external DEM.
- 2) Radiometric calibration to σ_0 , in order to enable the use of the backscatter coefficient as a classification feature.
- 3) Interferometric stack generation, providing all the possible combinations, both at VV and VH channels, between the SLC acquisitions in 2017.
- 4) Speckle filtering and coherence estimation. A boxcar filter with 19 samples in range and 4 samples in azimuth was employed for this purpose. This kernel size yields an output pixel resolution around $60 \text{ m} \times 80 \text{ m}$ (taking into account that the original image resolution was $3 \times 22 \text{ m}$ in range and azimuth, respectively). The resulting equivalent number of looks is 37 approximately. This number provides a good compromise between the loss of spatial resolution due to spatial averaging and the required accuracy in coherence estimation, since we expect to measure very low values of coherence at some dates, which would be severely overestimated if a small kernel size were employed [12].
- 5) Geocoding: all coherence and calibrated intensity data were finally geocoded into a common cartographic grid in UTM coordinates of size 1000×1000 pixels, so that the same geometry and pixel spacing of 20 m are used in both reference and satellite data.

For illustration purposes, Fig. 2 partially shows the temporal coherence matrix of the processed area (only the first 10 image pairs are shown). It is clearly observed that coherence progressively decreases as the temporal baseline (in days) between

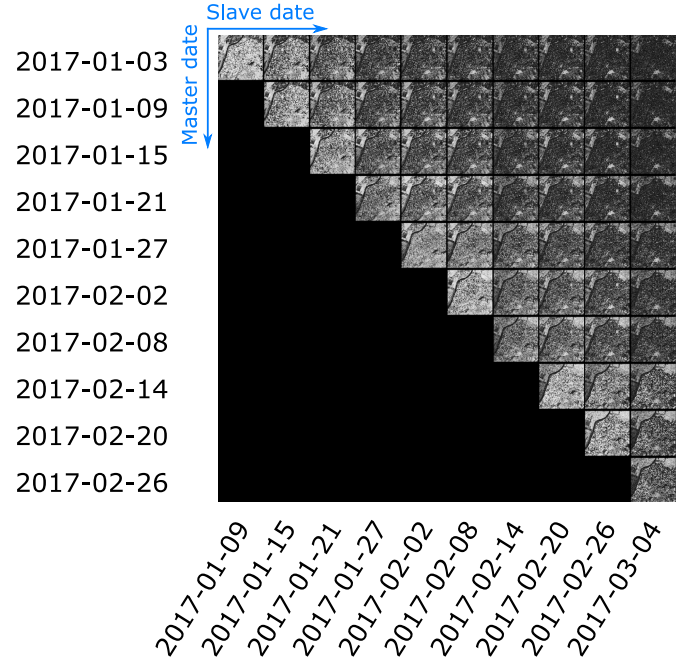


Fig. 2. Temporal coherence matrix of the processed area between 2017-01-03 and 2017-03-04. The polarimetric channel is VV.

master and slave pairs increases. In this work, we will only consider a short-baseline subset of the whole set of interferometric combinations. Specifically, coherence values coming from 6, 12, and 18 days of temporal baseline will be used as input features to the classification algorithm.

E. Classification Method and Evaluation

All the classification tests were carried out with the Random Forests (RF) classifier [13] using the implementation provided by the *scikit-learn* package in Python language. The classifier was run with the default parameters (e.g., number of trees equal to 100), and they were fixed for all the classification tests described in next section.

The process of splitting the whole input dataset into the training and testings sets represents a critical aspect of any supervised machine learning technique, since undesired effects such as overfitting (or overlearning) or biased classifications must be avoided. Due to the spatial filtering employed in the data preprocessing (boxcar of size 4×19), the values of the features at every pixel are correlated with those of adjacent pixels. Therefore, to avoid its influence on the classifier, an initial split was performed at field level: for each test, 50% of the fields of each crop type were selected for training and the remaining 50% of the fields were left for testing. This division of the original reference data is represented in Fig. 3.

The resulting number of fields and, hence, the number of pixels of each crop type, clearly varies among classes, showing that the training set [Fig. 3(a) and Table I] is imbalanced. This might be a problem concerning the accuracy of each individual class, since an overfitting toward majority classes (in this case, cotton, tomato, and sugar beet) is more likely to happen. To solve

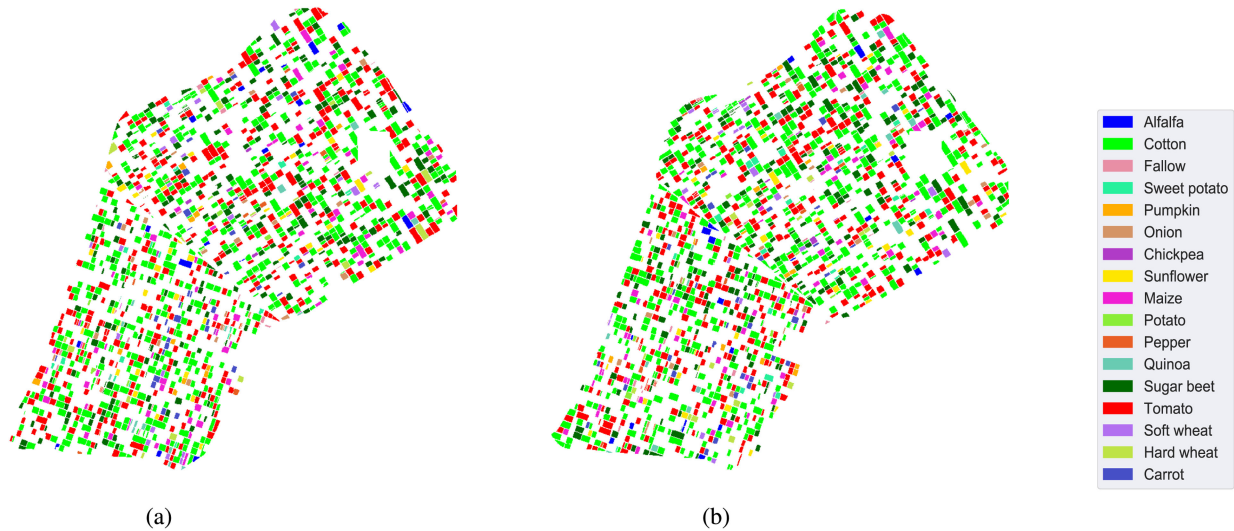


Fig. 3. Initial split of the reference data: for each crop type, half of the fields are used for training and the other half for testing. (a) Fields composing the training set. (b) Fields composing the testing set.

TABLE I
CHARACTERISTICS OF THE REFERENCE DATA SHOWING THE ORIGINAL NUMBER OF TRAINING AND TESTING SAMPLES OF EACH CROP TYPE AND THE TOTAL NUMBERS

Crop type	Initial training set		Testing set		Total	
	Number of fields	Number of samples	Number of fields	Number of samples	Number of fields	Number of samples
Cotton	560	53193	560	55918	1120	109111
Tomato	391	35511	391	35943	782	71454
Sugar beet	235	18523	236	19673	471	38178
Maize	72	6004	73	6260	145	12272
Sunflower	40	3226	41	3232	81	6458
Fallow	41	604	41	808	82	1404
Carrot	35	2315	36	2505	71	4820
Onion	30	1689	30	1749	60	3456
Soft wheat	22	1608	23	1738	45	3346
Sweet potato	21	1082	21	1697	42	2779
Alfalfa	20	1890	20	2106	40	3996
Hard wheat	18	1457	18	1982	36	3439
Pepper	16	680	17	744	33	1424
Quinoa	16	936	16	1470	32	2406
Pumpkin	13	975	13	1193	26	2168
Chickpea	11	388	11	437	22	825
Potato	7	388	8	512	15	900

this problem, the initial training set in Fig. 3(a) is subsampled so that all crop types have exactly the same number of training pixels. This number of pixels is provided by the minority class (i.e., the class presenting the smallest number of pixels) which is chickpea, as shown in Table I. The resulting subsampled training set is depicted in Fig. 4. Note that, with this strategy, each of the 17 classes gathers 388 pixels for training, so the total number of training samples represents around 2.5% of the total number of pixels of the reference data. It is also important to note that the selection of samples of the 16 classes which are not chickpea is performed randomly within the initial training fields.

For each classification test, once the model is trained, the evaluation is performed over the whole set of testing, which is formed by all pixels of the fields initially selected for testing (50% of the total fields). From the results obtained over the pixels in the testing data, the confusion matrix is computed and some

metrics are derived: overall accuracy (OA), Kappa coefficient, producer's accuracy (PA), and user's accuracy (UA) [14].

III. RESULTS

A. Inspection of the Input Features: Coherence and Backscattering Coefficient

Before running all classification tests, it is worth observing the temporal evolutions of all SAR observables that will be used as input features for classification. Fig. 5 shows the time-series of coherence values associated with every crop type throughout the whole year for both polarization channels, whereas Fig. 6 corresponds to backscatter coefficient. The locations of the fields are extracted from the reference set and, then, coherence and intensity values of each crop type are aggregated to produce a single mean and standard deviation for each date.

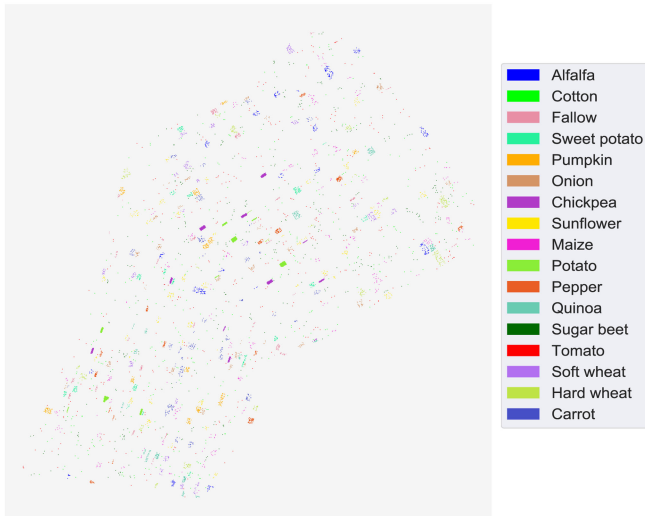


Fig. 4. Map of the subsampled dataset used for training.

By looking at Fig. 5, it is observed that, even though both channels exhibit a very similar evolution, channel VV always offers a larger coherence than channel VH. This is expected as a result of two aspects. First, the response from vegetated scenes in the cross-polar channel at C-band is expected to be more dependent on the vegetation layer than on the ground. As a consequence, VH polarization is more influenced by temporal decorrelation than VV. Second, VV channel is characterized by a higher backscattering level, which entails a higher signal-to-noise ratio (SNR) and, consequently, less decorrelation due to thermal noise [15].

The time-series of each crop type is closely related to its growing cycle. Accordingly, each crop type has its specific sowing, growing, and harvesting periods. These date intervals may be identified by means of the evolution of the coherence. In this regard, in the absence of vegetation (either because it has not been planted yet or because it has been harvested), higher coherence values are expected since parcels are bare fields, hence without temporal decorrelation. Conversely, as the crop is growing, a decrease in coherence is expected because the plants in the field are dynamically changing between consecutive observations, as well as due to weather effects on vegetation. This is easily verified by looking at Fig. 5(e), in which class fallow exhibits moderate to high coherence values throughout the whole year, whereas the rest of classes present periods of minimum coherence at some dates during the year. Moreover, it must be pointed out that the coherence is estimated using a finite spatial filter (4×19 boxcar) which is a biased estimator that overestimates more the lower values of coherence than the higher ones [12]. As a result, for all crop types, the minimum estimated coherence is just below 0.2, and coherence values smaller than that are not found.

Based on the previous reasoning, the calendar or growing period of every crop type can be identified in Fig. 5. For instance, sweet potato starts to grow in late May, since from this date, coherence progressively decreases until it reaches minimum values during summer (July–September). Then, coherence increases

after harvest in October. For most crop species, the interval with minimum coherence is different from the rest, which is a good sign for classification purposes. Unfortunately, in some cases, the time-series of coherence are very similar for several crops (e.g. cotton, sweet potato, pepper, and pumpkin), so confusion between these classes is expected.

Also, there are some isolated values of very low coherence, common to all crop types, in October and November. These drops were certainly caused by strong rain events which occurred during the fall of 2017 and which produce severe temporal decorrelation.

A similar analysis can be conducted on the time-series of backscattering coefficient represented in Fig. 6. As with coherence, intensity variations are due to the crop growing cycle. Even though intensities at both polarimetric channels exhibit globally similar trends along time, they are not as similar as the ones shown in Fig. 5 corresponding to VV and VH coherence, and some very clear differences between channels are locally observed. For instance, the response of VH channel differs from the one of VV channel for classes tomato (from May to September), carrot (from June to October), or soft wheat (from June to October), among others. These different responses were expected and are due to differences in the interaction of the waves involved at each polarimetric channel with vegetation (i.e. the scattering mechanisms present in the scene). Some of the crop types have been studied elsewhere with time-series of Sentinel-1 radiometric data, like wheat, maize, sugar beet, etc. [16]–[18], especially for monitoring purposes. Therefore, the physical causes of the radar responses for these crop species can be consulted in these references.

It is important to note that there are similarities between the temporal evolutions of both types of features: coherence and backscattering coefficient. More precisely, it is shown that coherence and intensity follow an inverse evolution in time. For instance, coherence of class cotton progressively starts to decrease in June and remains very low (around 0.2) until September, as shown in Fig. 5(a). Conversely, intensity data of this class increase from June to July and remain high until September, as shown in Fig. 6(a). The main reason of this behavior is the increase of backscattered signal when plants are present, which in turn decreases the coherence due to temporal decorrelation. In contrast, in absence of vegetation, the echoes from the bare ground show lower values but are more stable in time. Other classes, like sunflower, pepper, quinoa, and pumpkin, are clear examples of this opposite variation of coherence and intensity.

As a final comment, all the plots in Fig. 6 show clear peaks of intensity (at both channels) for some dates in February–April and October–December, which are clearly due to rain events which increased the soil moisture and, if plants were present, the water content in the vegetation volume. This is especially evident for fallow, for which a stable response would be expected along the whole year.

B. Classification Based on Coherence

The first test consists in training the RF model using all coherence values coming from the shortest temporal baseline

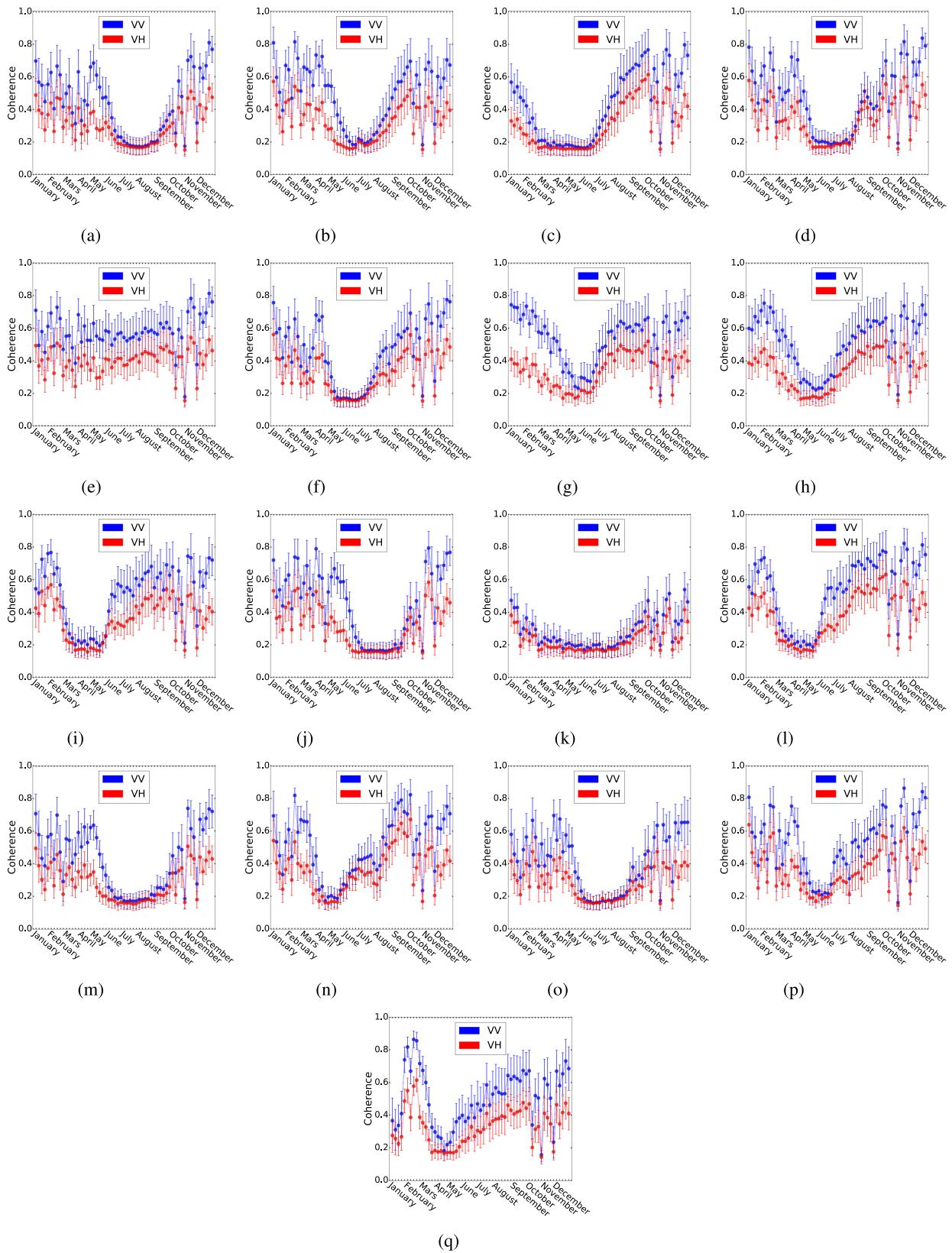


Fig. 5. Temporal evolution of the interferometric coherence at VV and VH channels. (a) Cotton. (b) Tomato. (c) Sugar beet. (d) Maize. (e) Fallow. (f) Sunflower. (g) Carrot. (h) Onion. (i) Soft wheat. (j) Sweet potato. (k) Alfalfa. (l) Hard wheat. (m) Pepper. (n) Quinoa. (o) Pumpkin. (p) Chickpea. (q) Potato.

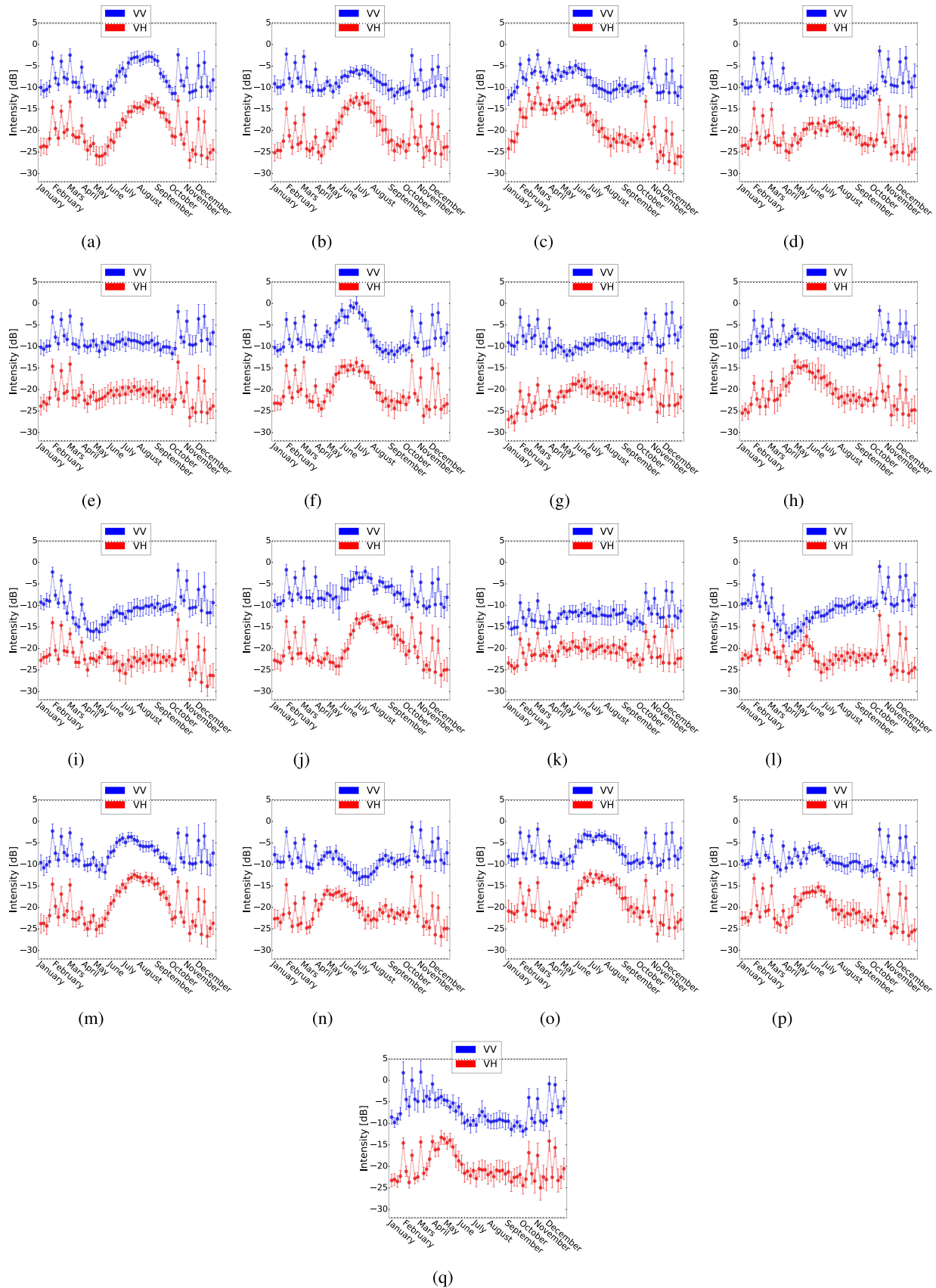


Fig. 6. Temporal evolution of the backscattering coefficient at VV and VH channels. (a) Cotton. (b) Tomato. (c) Sugar beet. (d) Maize. (e) Fallow. (f) Sunflower. (g) Carrot. (h) Onion. (i) Soft wheat. (j) Sweet potato. (k) Alfalfa. (l) Hard wheat. (m) Pepper. (n) Quinoa. (o) Pumpkin. (q) Chickpea. (r) Potato.

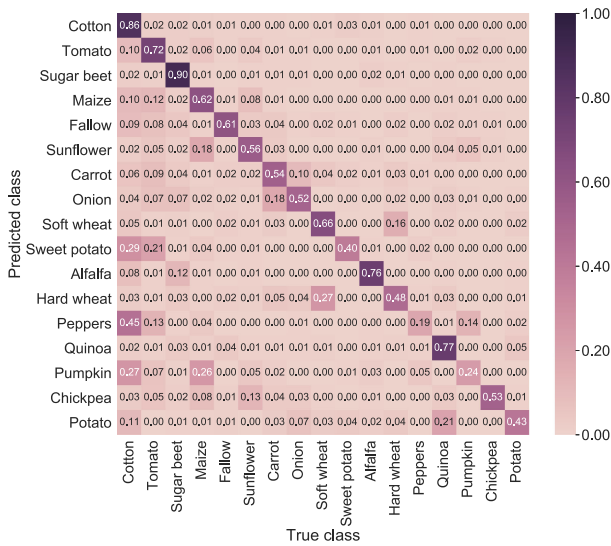


Fig. 7. Normalized confusion matrix obtained with the 6-day coherence at VV channel as input feature set.

TABLE II
ACCURACY ASSESSMENT OF THE RESULTS OBTAINED WITH THE 6-DAY COHERENCE AT VV CHANNEL

Crop type	Producer’s accuracy	User’s accuracy
Cotton	88.5%	85.9%
Tomato	88.2%	72.2%
Sugar beet	87.5%	90.0%
Maize	47.3%	62.2%
Fallow	31.8%	61.4%
Sunflower	43.1%	56.4%
Carrot	48.7%	54.1%
Onion	48.9%	52.2%
Soft wheat	51.6%	65.9%
Sweet potato	28.9%	39.7%
Alfalfa	47.3%	76.1%
Hard wheat	49.5%	48.0%
Pepper	12.0%	19.2%
Quinoa	59.9%	76.9%
Pumpkin	15.5%	23.9%
Chickpea	46.0%	53.3%
Potato	41.2%	41.2%
Overall accuracy	77.5%	
Kappa score	0.70	

(6 days) at VV polarization. Note that these results will be used as reference to evaluate the rest of options and combinations of input features. The resulting normalized confusion matrix is shown in Fig. 7, and the assessment metrics are presented in Table II.

It is observed that the overall accuracy is moderately high (77.5%). Crop types with the best classification scores are sugar beet, cotton, and tomato, with values of PA and UA from 80% to 90%, followed by a second large group of crop species with PA and UA which lie between 45% and 65%. Classes with the worst results are pepper and pumpkin (both worse than 25%), and sweet potato (below 40%). From the inspection of the confusion matrix and the time-series of coherence for these crop types (see Fig. 5), it is obvious that their responses are very similar

TABLE III
ACCURACY ASSESSMENT OF THE RESULTS OBTAINED SEPARATELY WITH THE 12-DAY AND 18-DAY COHERENCE AT VV CHANNEL

Crop type	Temporal baselines			
	12 days		18 days	
	PA	UA	PA	UA
Cotton	86.0%	81.1%	85.3%	77.6%
Tomato	87.6%	60.7%	88.1%	65.8%
Sugar beet	83.4%	86.8%	79.3%	81.4%
Maize	47.2%	59.4%	37.0%	49.1%
Fallow	30.1%	58.8%	33.1%	54.4%
Sunflower	36.9%	52.7%	29.1%	48.2%
Carrot	48.6%	52.5%	48.8%	52.8%
Onion	43.7%	51.8%	33.8%	52.5%
Soft wheat	54.5%	72.6%	46.9%	66.9%
Sweet potato	26.6%	44.2%	18.2%	36.9%
Alfalfa	33.9%	70.6%	26.5%	66.5%
Hard wheat	41.2%	39.4%	31.2%	30.6%
Pepper	8.1%	15.9%	8.7%	17.1%
Quinoa	51.1%	68.2%	42.7%	69.5%
Pumpkin	8.6%	14.6%	3.8%	7.3%
Chickpea	39.4%	28.1%	19.3%	16.0%
Potato	21.4%	31.8%	27.0%	37.7%
OA	73.8%	OA	69.7%	
Kappa	0.66	Kappa	0.60	

and are also similar to cotton. so that the classifier is unable to properly distinguish them. Consequently, since the training set was appropriately prepared to avoid overfitting and class imbalance, we conclude that classification inaccuracies are only due to the input features.

1) *Influence of the Temporal Baseline:* Besides using 6-days coherence, the two second shortest temporal baselines (12 and 18 days) will be also evaluated, both individually and combined, so as to check if a further gain is obtained when including more data.

First, we apply the classifier using 12- and 18-day coherence individually as input features, and only at VV channel as in the previous example. Table III shows the results of these two cases. It is easily appreciated that the classification accuracy (in terms of PA and UA) of most classes decreases progressively as the temporal baseline increases. For instance, the UA of alfalfa goes down from 76% (6 days) to 71% (12 days) and to 67% (18 days). In some cases, this decrease is even more pronounced, as for chickpea, whose UA goes from 53% (6 days) to 28% (12 days) and to 16% (18 days). For a few crop types, like maize, their PA or UA is maintained from 6 to 12 days, but then they decrease clearly at 18 days; and in the case of carrot, its PA and UA are mostly independent of the temporal baseline. Finally, user accuracies of soft wheat and sweet potato are higher at 12 days than at 6 days, but then they notably decrease at 18 days.

In summary, a generalized loss of accuracy is obtained when coherence coming from longer temporal baselines is used. This is certainly caused by the higher level of decorrelation which is present in coherence images (clearly visible in Fig. 2) generated with image pairs with longer baselines, which degrade the quality of interferometric data. In the overall metrics, OA decreases from 77.5% at 6 days (see Table II), to 73.8% at 12 days and to 69.7% at 18 days, i.e., around 4% at each step.

TABLE IV
ACCURACY ASSESSMENT OF THE RESULTS OBTAINED JOINTLY WITH THE COHERENCE FROM THE FIRST TWO AND FIRST THREE SHORTEST TEMPORAL BASELINES AT VV CHANNEL

Crop type	Temporal baselines			
	6 and 12 days		6, 12 and 18 days	
	PA	UA	PA	UA
Cotton	88.3%	85.0%	87.6%	84.4%
Tomato	89.4%	72.6%	88.6%	71.6%
Sugar beet	86.7%	89.6%	86.1%	90.0%
Maize	47.6%	64.0%	48.5%	63.4%
Fallow	30.3%	62.5%	33.6%	61.1%
Sunflower	43.0%	55.9%	42.2%	55.7%
Carrot	53.0%	52.5%	54.4%	55.7%
Onion	48.3%	55.3%	48.8%	56.1%
Soft wheat	49.5%	69.2%	52.8%	69.1%
Sweet potato	28.3%	45.1%	25.9%	43.0%
Alfalfa	45.5%	73.6%	42.9%	72.6%
Hard wheat	44.9%	39.1%	46.2%	41.9%
Pepper	12.6%	21.6%	15.0%	21.4%
Quinoa	61.4%	74.4%	56.9%	78.7%
Pumpkin	12.7%	19.1%	8.5%	13.4%
Chickpea	37.6%	34.5%	44.4%	37.5%
Potato	38.6%	54.3%	34.6%	43.4%
	OA	77.2%	OA	76.7%
	Kappa	0.70	Kappa	0.69

Another relevant test consists in incorporating sets of different temporal baselines to the classification process, that is, to simultaneously use coherence data coming from both 6 and 12 days, and also 6, 12, and 18 days. The resulting accuracy metrics are shown in Table IV, in which we observe that the overall variation between these two cases and the one with only 6-day coherence is very small.

At class level, the most extreme changes at UA and PA are below 5%, but in most cases, they are below 2%. In fact, the inclusion of the second temporal baseline (and also the third) does not improve the global accuracy with respect to the shortest temporal baseline. This lack of improvement is a consequence of the lower quality of the coherence measured with longer temporal baselines, due to increased temporal decorrelation, as it was verified in their individual results (Table III).

2) *Influence of Polarization*: Sentinel-1 provides dual-pol images routinely over land from channels VV and VH, so it is worth testing the performance of both polarimetric channels as input features to the classifier.

Table V presents the accuracy scores obtained by individually employing 6-day coherence of VH polarization. A decrease of accuracy is found for all classes with respect to the results of the VV channel (Table VIII), with losses of 5%–15% in PA and UA for most crop types, and important drops (more than 20%) for chickpea and potato. Only for quinoa (PA and UA) and maize (PA) their scores are just 1%–3% below the results at VV channel. Moreover, the global accuracy decreases from 77.5% to 69.1% and the Kappa score from 0.70 to 0.60, showing that VH coherence performs clearly worse than VV one with the same baseline configuration (6 days). This was expected as a consequence of the lower SNR present in VH data, as previously stated.

TABLE V
ACCURACY ASSESSMENT OF THE RESULTS OBTAINED WITH THE 6-DAY COHERENCE AT VH CHANNEL

Crop type	Producer's accuracy	User's accuracy
Cotton	85.2%	78.7%
Tomato	81.8%	60.8%
Sugar beet	83.2%	84.6%
Maize	49.3%	58.8%
Fallow	24.8%	47.6%
Sunflower	26.7%	37.9%
Carrot	37.0%	44.5%
Onion	29.7%	38.8%
Soft wheat	43.9%	66.3%
Sweet potato	14.3%	38.8%
Alfalfa	28.3%	71.0%
Hard wheat	36.5%	42.2%
Pepper	7.7%	19.4%
Quinoa	58.0%	48.4%
Pumpkin	6.6%	17.0%
Chickpea	12.9%	9.8%
Potato	22.9%	16.8%
Overall accuracy	69.1%	
Kappa score	0.60%	

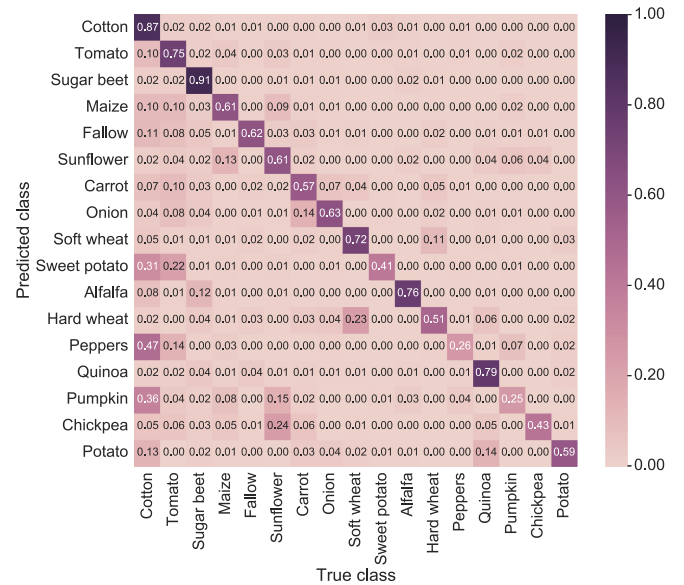


Fig. 8. Normalized confusion matrix obtained with the 6-day coherence at both VV and VH channels as joint input feature set.

However, a more complete evaluation of the contribution of the dual-pol acquisition mode of Sentinel-1 consists in checking whether the combination of both polarizations (VV and VH) as input features yields an additional gain in the crop-type classification performance. Additionally, all temporal baselines are considered and compared to check if increasing the amount of inputs (three baselines and two polarimetric channels) improves the accuracy. The normalized confusion matrix obtained with the 6-day coherence is shown in Fig. 8, and Table VI presents all class-level and overall accuracy metrics for three combinations of baselines: 6-day alone, 6- and 12-day, and 6-, 12-, and 18-day coherence.

Compared to the confusion matrix provided by the 6-day coherence at VV alone (see Fig. 7), Fig. 8 evidences a better

TABLE VI
ACCURACY ASSESSMENT OF THE RESULTS OBTAINED WITH THE COHERENCE FROM THE FIRST TWO AND FIRST THREE SHORTEST TEMPORAL BASELINES AT BOTH VV AND VH CHANNELS SIMULTANEOUSLY

Crop type	Temporal baselines					
	6 days		6 and 12 days		6, 12 and 18 days	
	PA	UA	PA	UA	PA	UA
Cotton	88.1%	87.0%	87.6%	86.4%	87.8%	85.9%
Tomato	89.0%	74.5%	89.2%	73.7%	89.3%	74.5%
Sugar beet	87.0%	90.8%	86.7%	90.3%	85.7%	90.1%
Maize	58.2%	61.3%	57.5%	63.8%	58.3%	65.7%
Fallow	32.7%	61.6%	32.8%	61.2%	34.6%	61.4%
Sunflower	44.6%	60.8%	45.3%	59.9%	46.3%	58.5%
Carrot	53.5%	57.2%	55.8%	56.3%	57.4%	57.4%
Onion	58.0%	62.9%	57.3%	61.5%	56.8%	64.0%
Soft wheat	55.3%	72.5%	56.0%	73.6%	50.4%	76.2%
Sweet potato	29.6%	40.7%	30.8%	46.7%	27.6%	41.7%
Alfalfa	48.3%	76.2%	44.6%	75.9%	43.5%	75.4%
Hard wheat	53.7%	50.9%	57.7%	50.0%	56.3%	40.3%
Pepper	17.4%	25.5%	16.4%	21.9%	20.0%	25.2%
Quinoa	64.4%	78.9%	63.1%	77.8%	60.5%	76.7%
Pumpkin	18.3%	25.0%	15.9%	25.7%	14.4%	22.4%
Chickpea	39.3%	43.2%	38.4%	31.6%	50.3%	41.4%
Potato	54.5%	59.2%	43.4%	49.8%	42.7%	48.8%
	OA	79.2%	OA	78.7%	OA	78.5%
	Kappa	0.73	Kappa	0.72	Kappa	0.71

result for almost all crop types when dual-pol data are used. While the accuracy of predominant classes remains high (for instance, it barely varies for cotton, tomato, and sugar beet), other classes are better identified. For instance, the UA values for classes carrot, onion, and soft wheat increase, respectively, from 54%, 52%, and 66% (when single polarization VV is used) to 57%, 63%, and 72% when both channels are processed jointly. It is found that the best global accuracy obtained so far, which was 77.5% when using channel VV and the shortest temporal baseline, has improved to 79.2% when both polarizations are exploited and the same 6-day baseline is used. Analogously, Kappa score has increased from 0.70 to 0.73.

Unfortunately, the inclusion of the coherence from the other two baselines (12 and 18 days) along with the additional polarization does not have a significant impact on the accuracy. This is in line with the results shown in Section III-B1, where data from additional baselines were added to the single-pol (VV) and shortest-baseline coherence. In fact, the best final results are obtained when the shortest temporal baseline (6 days) is exploited individually. The addition of extra baselines produces a progressive decrease of the performance of the classifier, especially in the PA and UA of some classes, despite the difference in the global scores is very small: 79.2%, 78.7%, and 78.5% in terms of OA, and 0.73, 0.72, and 0.71 in terms of Kappa score.

C. Classification Based on Intensity

The same analysis has been repeated using only the backscattering coefficient provided by the images as input features. Note that this corresponds to the traditional approach for crop-type mapping with time-series of radar data.

1) *Influence of the Quantity of Images*: The first test consists in evaluating the influence the quantity of available images has in the classification process. This can be regarded as a

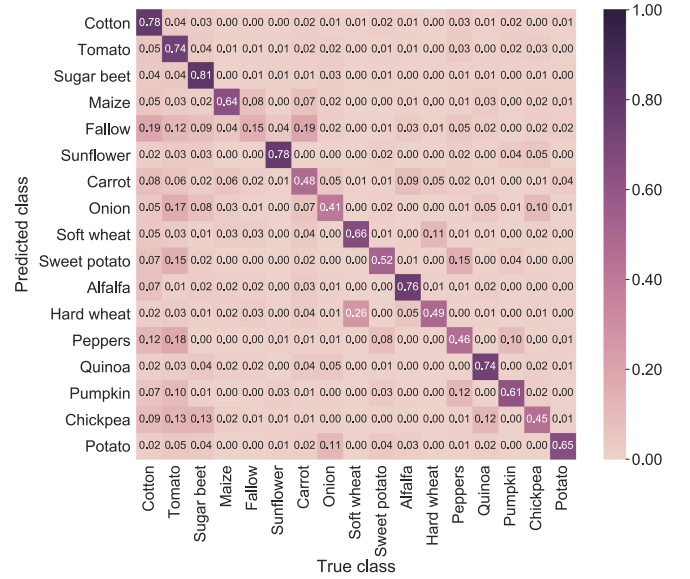


Fig. 9. Normalized confusion matrix obtained with all 60 backscatter images at the VV channel as input feature set.

TABLE VII
ACCURACY ASSESSMENT OF THE RESULTS OBTAINED WITH THE BACKSCATTERING COEFFICIENT AT VV CHANNEL USING DIFFERENT AMOUNTS OF IMAGES

Crop type	Number of images					
	60 images (6 days)		30 images (12 days)		20 images (18 days)	
	PA	UA	PA	UA	PA	UA
Cotton	91.7%	78.3%	91.5%	73.6%	90.4%	71.8%
Tomato	84.6%	73.5%	82.4%	69.2%	82.7%	64.5%
Sugar beet	81.8%	81.5%	80.2%	77.0%	80.3%	74.5%
Maize	80.0%	63.8%	69.5%	59.6%	58.5%	56.5%
Fallow	7.0%	17.9%	4.7%	17.3%	3.4%	15.0%
Sunflower	73.7%	77.2%	66.6%	76.5%	58.4%	74.8%
Carrot	30.2%	48.5%	28.2%	46.4%	25.8%	40.6%
Onion	24.6%	42.2%	17.8%	33.4%	16.9%	31.5%
Soft wheat	55.7%	72.5%	48.4%	60.5%	48.2%	60.1%
Sweet potato	31.4%	66.1%	19.7%	48.7%	14.5%	42.4%
Alfalfa	57.5%	53.1%	54.4%	74.5%	50.3%	72.1%
Hard wheat	55.5%	76.2%	47.6%	45.9%	48.1%	50.4%
Pepper	8.5%	48.7%	6.7%	43.8%	4.0%	32.5%
Quinoa	49.0%	72.2%	40.0%	65.8%	38.7%	59.7%
Pumpkin	20.3%	61.9%	15.1%	49.7%	14.2%	46.3%
Chickpea	9.3%	43.7%	8.4%	38.7%	5.8%	32.3%
Potato	30.2%	65.2%	27.3%	51.0%	21.6%	50.4%
	OA	74.2%	OA	69.8%	OA	67.0%
	Kappa	0.66	Kappa	0.61	Kappa	0.58

similar test as the one shown in Section III-B1 concerning the temporal baseline between a pair of images used to compute the coherence.

As in Section III-B, results obtained with all available images (60) at VV polarization are used as reference. Fig. 9 shows the normalized confusion matrix obtained in this case and the corresponding accuracy scores are shown in the first column of Table VII. In general terms, the results are slightly worse than the ones obtained with coherence in the same configuration, since now the OA is 74.2%, instead of 77.5% (see Table II). However, the classification performance for the individual crops is quite different in most cases with respect to the results based

TABLE VIII
ACCURACY ASSESSMENT OF THE RESULTS OBTAINED WITH ALL 60
BACKSCATTER IMAGES AT VH CHANNEL

Crop type	Producer's accuracy	User's accuracy
Cotton	94.6%	75.4%
Tomato	91.5%	74.9%
Sugar beet	82.3%	90.6%
Maize	72.2%	65.5%
Fallow	10.8%	30.8%
Sunflower	40.1%	62.5%
Carrot	49.2%	61.5%
Onion	48.6%	60.5%
Soft wheat	65.3%	65.2%
Sweet potato	29.7%	62.5%
Alfalfa	56.3%	68.9%
Hard wheat	60.8%	64.2%
Pepper	6.5%	52.3%
Quinoa	56.8%	73.6%
Pumpkin	16.1%	55.6%
Chickpea	9.9%	31.8%
Potato	23.7%	69.7%
Overall accuracy	75.2%	
Kappa score	0.68	

on coherence. For instance, the PA with intensity data for maize and sunflower is 80% and 73%, instead of 47% and 43%, respectively, obtained with coherence, so these crop types are much better classified now. The best classified crops are the same ones (cotton, tomato, and sugar beet) and provide accuracies in the same order as with the coherence. On the other extreme, carrot, onion, chickpea, and fallow perform much worse when intensity is exploited than when coherence is used. This heterogeneous comparison between the results with coherence and intensity is a positive sign for their combined used as input features, as it will be analyzed in Section III-D.

Since the whole dataset consists of 60 images acquired every 6 days (as previously mentioned), using one-half and one-third of images (namely one every two, and one every three images) directly yields one image every 12 and 18 days, respectively. The results provided by employing only these subsets of images are illustrated in Table VII. It is clearly observed that the accuracy progressively decreases for all classes when less images are considered. OA decreases to 69.8% with one-half of the images and to 67% with one-third of the images. At crop-type level, the best classified ones are the least affected, but others, like maize, wheat, quinoa, etc. suffer progressive drops greater than 5% in PA and/or UA.

2) *Influence of Polarization*: The contribution of the dual-pol acquisitions in crop-type mapping, using backscattering coefficient as input feature, has been studied in the past [19]–[23]. It is known that the cross-polar channel backscattering is more sensitive to vegetation than the co-polar one. Consequently, VH polarization has shown to perform better than HH or VV channels for crop classifications.

Results obtained using all 60 intensity images of VH polarization are illustrated with the confusion matrix shown in Fig. 10, and accuracy metrics are summarized in Table VIII. In our test, the OA provided by the VH channel is 75.2%, only 1% better than the VV channel. However, some crop types that were

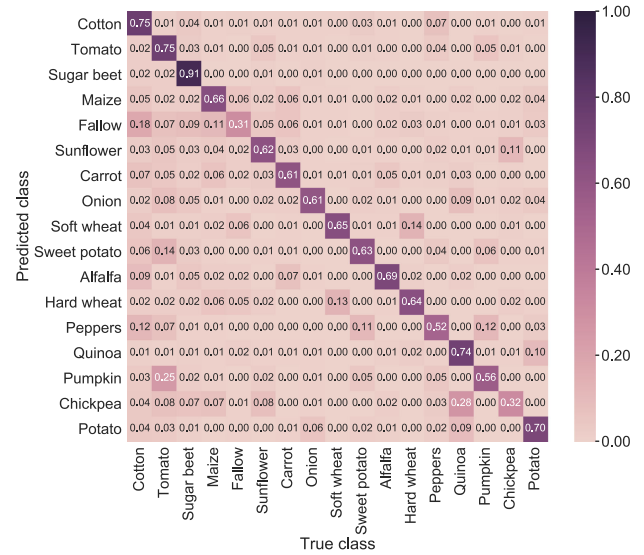


Fig. 10. Normalized confusion matrix obtained with all 60 backscatter images at the VH channel as input feature set.

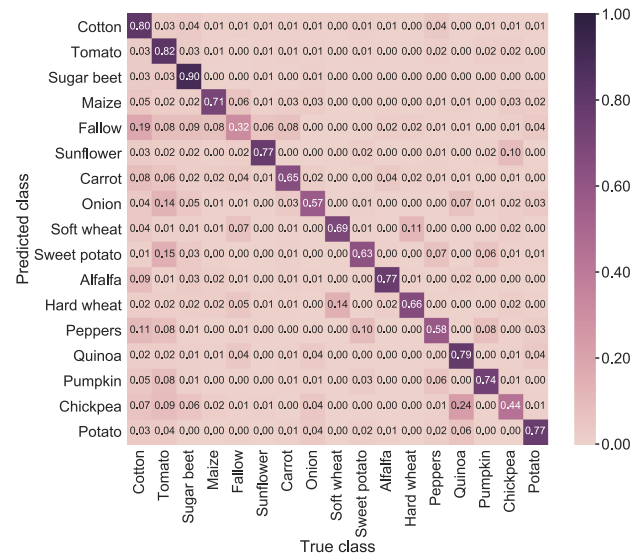


Fig. 11. Normalized confusion matrix obtained with all 60 backscatter images at both VV and VH channels as joint input feature set.

poorly identified with the VV backscatter exhibit an increase of accuracy with VH images. For instance, the UA of carrot, onion, and hard wheat is improved from 48%, 41%, and 49% (with VV images) to 61%, 61%, and 64% (with VH images), respectively. Conversely, other classes suffer notable decreases of accuracy, like sunflower (PA equal to 40% with VH instead of 73% with VV).

As with coherence, we have also evaluated the joint exploitation of both channels (VH and VV intensity images) as input set to the classifier. The resulting confusion matrix is represented in Fig. 11 and accuracy scores are detailed in Table IX. By comparing the main diagonals of confusion matrices of Fig. 10 (with VH alone) and 11 (with both VV and VH), it is deduced

TABLE IX
ACCURACY ASSESSMENT OF THE RESULTS OBTAINED WITH ALL 60
BACKSCATTER IMAGES AT BOTH VV AND VH CHANNELS AS
JOINT INPUT FEATURE SET

Crop type	Producer's accuracy	User's accuracy
Cotton	93.8%	80.1%
Tomato	90.1%	82.3%
Sugar beet	83.1%	89.7%
Maize	80.0%	71.5%
Fallow	9.7%	31.6%
Sunflower	75.6%	76.9%
Carrot	53.9%	65.1%
Onion	43.1%	56.8%
Soft wheat	66.5%	69.0%
Sweet potato	46.2%	62.8%
Alfalfa	64.4%	77.0%
Hard wheat	69.7%	66.2%
Pepper	11.3%	57.9%
Quinoa	63.0%	78.6%
Pumpkin	32.2%	73.6%
Chickpea	10.2%	43.9%
Potato	29.4%	76.7%
Overall accuracy	80.0%	
Kappa score	0.73	

that the accuracy of almost all classes is improved and there is generally less confusion.

This enhancement of the classification performance is clear in the PA and UA of most crops (see Table IX). For instance, the final UA of nine crop types is above 70%, and there are only two classes (fallow and chickpea) below 50%. From the global point of view, the use of both polarizations provides an increase of almost 5% of OA (from 75.2% to 80.0%), and a gain of 0.05 in terms of Kappa score (from 0.68 to 0.73) with regard to using VH data only, which is quite remarkable.

Finally, is important to note that coherence and intensity data provide very similar global accuracies when used individually with dual-pol data (i.e., exploiting both VV and VH). They provide the same Kappa score (0.73) and almost the same OA (79.2% with coherence and 80.0% with intensity) as shown in Tables VI and IX.

Concerning class-level accuracies, some classes which are poorly identified with coherence data are better classified when intensity data are used, and vice versa. For instance, the UA of pepper and pumpkin is around 25% with coherence data, but 58% and 74%, respectively, when intensity data are used instead. Conversely, fallow, which is poorly classified with intensity (PA 10%, UA 32%), presents much better results with the coherence (PA 33%, UA 62%). Therefore, both types of products could be used in a complementary way to improve classification accuracy.

D. Classification Based on Coherence and Intensity

The final evaluation of Sentinel-1 data performance for crop-type mapping consists in using as input both the time-series of coherence and intensity data. The analysis carried out in Sections III-B and III-C proves that coherence values coming from the shortest temporal baseline (6 days) and all intensity images (1 image every 6 days) provide the best classification

TABLE X
ACCURACY ASSESSMENT OF THE RESULTS OBTAINED WITH ALL 60
BACKSCATTER IMAGES AND 6-DAY COHERENCE

Polarisation	VV		VH		VV + VH	
	PA	UA	PA	UA	PA	UA
Cotton	93.7%	87.7%	94.9%	83.5%	95.1%	87.9%
Tomato	90.2%	84.9%	91.2%	79.6%	92.1%	87.4%
Sugar beet	89.9%	94.1%	86.7%	93.1%	89.1%	94.5%
Maize	79.9%	81.6%	77.5%	79.9%	82.2%	81.8%
Fallow	31.2%	63.8%	27.1%	51.6%	31.8%	60.7%
Sunflower	81.0%	82.4%	46.4%	66.2%	80.2%	81.2%
Carrot	63.2%	67.5%	64.0%	69.1%	68.7%	74.4%
Onion	52.1%	65.5%	51.1%	67.3%	53.7%	73.2%
Soft wheat	68.7%	76.7%	72.9%	76.0%	76.1%	78.6%
Sweet potato	55.5%	56.5%	37.9%	63.0%	59.9%	62.8%
Alfalfa	69.2%	84.5%	60.7%	77.5%	73.7%	84.0%
Hard wheat	69.5%	58.6%	75.7%	67.9%	79.8%	72.1%
Pepper	18.7%	50.8%	12.6%	54.0%	22.6%	64.5%
Quinoa	76.3%	86.8%	68.7%	80.1%	25.2%	88.4%
Pumpkin	34.5%	66.6%	20.4%	56.4%	42.3%	74.4%
Chickpea	42.3%	65.0%	17.1%	32.9%	25.2%	54.2%
Potato	48.2%	74.0%	32.6%	69.3%	44.9%	78.7%
OA	85.4%	81.5%	86.7%	83.0%	86.7%	83.0%
Kappa	0.81	0.76	0.83	0.76	0.83	0.83

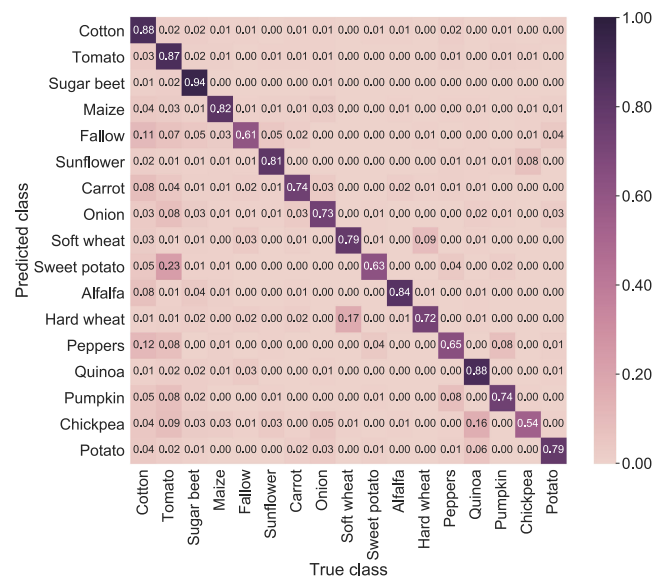


Fig. 12. Normalized confusion matrix obtained with all 60 backscatter images and 6-day coherence at both VV and VH channels.

results, respectively. Therefore, here we use directly all intensity images, and coherence values coming from temporal baselines longer than 6 days are not considered. For completeness, the influence of polarization is also studied by analyzing the results of the individual channels and their combination.

The resulting accuracy scores are detailed in Table X, and the confusion matrix for the dual-pol case is also shown in Fig. 12. The first obvious comment is that, regardless of polarization, the use of both types of features clearly outperforms the results obtained with only one type of data (either coherence or intensity). The increase in OA with respect to any of the equivalent cases with only coherence or intensity ranges from 6% to 8%,

reaching 86.7% when both polarimetric channels are considered (the highest OA was 79.2% using dual-pol coherence and 80.0% using the intensity of both channels). Moreover, Kappa score reached 0.83, which showed a remarkable increase with respect to the previous best cases (0.73).

The improved overall metrics are in line with significant improvements in accuracy at class level. For instance, the UA of cotton, tomato, sugar beet, and maize increases, respectively from 86%, 72%, 90%, and 62% using only VV coherence, or from 75%, 75%, 91%, and 66% using VV intensity, to 88%, 85%, 94%, and 82% when both products are employed. In fact, and also regardless of polarization, all classes present now UA higher than 50%, except chickpea with VH data only, whose UA is 33%.

Furthermore, VV data clearly provide better classification results than VH data, as shown in Table X. However, the best classification results are again obtained when both polarizations are used (i.e., coherence and intensity of VV and VH channels). As shown in Fig. 12, confusion among classes is lower. With VV and VH, 13 of the 17 classes exhibit UA higher than 70%, and the minimum UA is 54%.

Finally, these results prove that coherence and intensity data are undoubtedly complementary for this application. Classes which were poorly classified with any of the two features, such as pepper and pumpkin (UA around 25%) with dual-pol coherence, and fallow and chickpea (UA equal to 32% and 44%, respectively) with dual-pol intensity images, present increased accuracies with both features: UA equal to 65% for pepper, 74% for pumpkin, 61% for fallow, and 54% for chickpea.

IV. DISCUSSION

The results obtained in this work can be compared with those obtained in previous experiments with time-series of SAR data, and more specifically with Sentinel-1 data, e.g. [3], [4], but always taking into account that each study about crop-type mapping has unique characteristics, including the number and specificity of crop species present in the study site, the cultivation practices, the agro-climatic conditions, which usually depend on the geographical location, and the dates and time span of the acquisitions. This complicates comparison in absolute terms and has to be considered to draw right conclusions. For instance, the time span covered by the satellite images in this work is a whole year, with data from a single orbit, whereas only 4 months were used in [3], and more than one year and three orbits were exploited in [4].

Provided that the objective of this work is to assess the contribution of Sentinel-1 interferometric coherence to crop-type mapping, it is important to quantify the added value of the sets of input features that include interferometric coherence with respect to those that do not consider it. In this sense, it has been demonstrated for the first time that the addition of time-series of Sentinel-1 coherence improves the OA (more than 6% in our site) with respect to the best case based only on time-series of the backscattering coefficient, reaching 86.7% when the two polarimetric channels are exploited. By observing the time-series of

TABLE XI
ACCURACY ASSESSMENT OF THE RESULTS OBTAINED WITH SINGLE INTERFEROMETRIC PAIRS AS A FUNCTION OF THE MONTH

Month	Overall accuracy	Kappa score
January	16.5%	0.10
February	18.7%	0.12
March	23.1%	0.16
April	27.9%	0.19
May	35.8%	0.26
June	32.9%	0.24
July	34.6%	0.25
August	33.8%	0.24
September	28.8%	0.19
October	18.4%	0.10
November	10.1%	0.03
December	10.2%	0.03

Coherence and backscatter images at both VV and VH channels are used as input feature set for each pair.

interferometric coherence measured for all crop types in this site, we conclude that the growing season of most species coincides with a period of very low coherence. Before the early vegetative stages and after harvest, the coherence values are significantly higher, so the crop calendar is well identified by the coherence magnitude. The detection of harvest date by means of Sentinel-1 coherence was first demonstrated in [18] for some crops. Despite the growing season is also clearly identified in the time-series of backscatter, this study has demonstrated that coherence provides additional information to better capture the features of the crops, hence improving the classification performance. A similar conclusion has been obtained recently in [11] by using TanDEM-X repeat-pass coherence values, despite the increased temporal baseline (11 days instead of 6 days) and a much shorter time span (3 months instead of a whole year). Clearly, the quite different response of coherence in the presence and absence of vegetation, as well as the influence of crop structure on it, provides the extra information required to enhance the classification performance.

The previous comment opens also the discussion about the advantage of using time-series of coherence data instead of single coherence data for crop-type mapping. With other types of input features (e.g. backscatter and polarimetry), the advantage of time-series is evident in crop classification [23]. However, it is worth testing the performance of single interferometric pairs for the same purpose. Table XI shows the overall scores obtained by using a single interferometric pair, which was selected as the first of each month in order to study also the influence of the crop calendar on it. For each case, the input data is composed of six features: coherence of the pair and backscatter coefficient of the two images of the pair, and for the two polarimetric channels. Obviously, the results are really poor from the practical point of view, with OA values always below 40%. The best months in this approach are from May to August, which are the only ones providing an OA above 30%. In this test site, most of the crops are sown in spring and summer, so these months coincide with the early growing stages of most crops, which are captured by the coherence data, thanks to temporal decorrelation, and by backscatter due to the increased response in the presence of

vegetation. In summary, as expected, the availability of one-year long time-series of Sentinel-1 data, with short revisit time and without missing acquisitions, provides the amount information required to distinguish among the crop types present in this region.

Finally, it is also worth comparing the results found in this work on crop-type mapping with those obtained in [9] on land-cover classification. With the shortest temporal baseline available in that work (12 days) and using the same classifier (RF), the OA values obtained in three different sites ranged from 65% to 74% using only coherence at the two channels. The OA increased from 74% with coherence alone to 80% when both coherence and intensity were used (and employing both polarimetric channels), but it was only tested in one test site. The equivalent case in the present work, but with a 6-day baseline, yields 79% of OA with coherence alone and 86.7% by employing coherence and intensity. Despite the limited comparability between cases, in both results, the contribution of the time-series of Sentinel-1 coherence is clear and in a similar amount. The consistency of this contribution in land cover classification was demonstrated in [9] by testing many different classifiers and evaluation strategies, including at pixel and object level, with and without segmentation. Consequently, it can be stated that its equivalent contribution in crop-type mapping is also consistent and independent from the specific classification algorithm.

V. CONCLUSION

This work investigates the potential of Sentinel-1 interferometric and radiometric data for generating thematic maps of crop types. First, it is shown that both types of features exhibit very remarkable and similar results when used individually. Overall classification accuracies lie between 70% and 80%, depending on the input dataset used by the classifier. In this regard, concerning coherence data, it is proved that the shortest temporal baseline coherence (6 days) clearly provides the best classification results, showing the enhanced performance the two-satellite constellation offers for this application. In fact, the inclusion of coherence data coming from longer temporal baselines has a negative impact on the results. Regarding intensities, we have shown that using more images (1 every 6 days) provides higher classification accuracies, proving again the advantage of the revisit time of 6 days of Sentinel-1.

Second, we have analyzed the impact of polarization. Concerning coherence, using the data of the VV channel as input yields better results than using the one of the VH counterpart. This was expected because of the higher SNR and smaller temporal decorrelation of VV with respect to VH, which makes them less noisy. Conversely, VH intensity performs slightly better than the VV one, due to the higher sensitivity to vegetation of VH, as it was previously studied in literature. However, the important aspect of polarization is that the behavior of both channels is somehow complementary, since jointly using the data of both polarizations as input to the classifier improves the quality of the classification.

Third, an important conclusion of this work is that coherence and intensity data are indeed complementary for this application.

It is shown that when both features are jointly used as input to the classifier, there is a very significant increase in accuracy, which becomes even higher if both polarimetric channels are exploited, reaching an overall classification accuracy equal to 86.7%. Obviously, the use of both channels for intensity and interferometry entails a high computational burden. In this regard, if some degradation of performance is acceptable, the exploitation of the VV channel alone provides results only slightly worse (OA equal to 85.4%) than in the dual-pol case.

Finally, some directions for future research are also proposed. The selection of the multilook filter employed in this work (boxcar) was done on the basis of the simplest processing, at the expenses of degraded resolution and, hence, potential problems in edges between fields and/or when parcels are very small. In this regard, recent works exploiting Sentinel-1 backscatter data have observed worse performances for small parcels than for large ones [3], [4]. Therefore, the use of more sophisticated filtering techniques, like nonlocal approaches [24], should be tested for the computation of both coherence and intensity. In addition, more experiments over different geographical areas and/or where other crop types are present should be carried out to further confirm the results obtained in this work. The use of interferometric coherence as input feature for crop-type mapping by unsupervised classification approaches is also an interesting study to be carried out for measuring its specific performance in this application with such a type of classifiers. In the same vein, the potential as input to supervised deep learning classifiers constitutes also a future line of research, since there are variants of this technique in specially adapted to the analysis and exploitation of multitemporal data.

ACKNOWLEDGMENT

The reference data were provided by the Regional Government of Andalucía and the Spanish Agrarian Guarantee Fund (FEGA). The authors would like to thank Elena Navarro (FER-AGUA), María P. González-Dugo (IFAPA), and Luciano Mateos (IAS-CSIC) for the helpful discussions about the particular features of the test site and on the final applications of this study.

REFERENCES

- [1] D. Bargiel, "A new method for crop classification combining time series of radar images and crop phenology information," *Remote Sens. Environ.*, vol. 198, pp. 369–383, 2017.
- [2] B. Kipkemboi Kenduuiwo, D. Bargiel, and U. Soergel, "Crop-type mapping from a sequence of Sentinel 1 images," *Int. J. Remote Sens.*, vol. 39, no. 19, pp. 6383–6404, 2018.
- [3] E. Tomppo, O. Antropov, and J. Praks, "Cropland classification using Sentinel-1 time series: Methodological performance and prediction uncertainty assessment," *Remote Sens.*, vol. 11, no. 21, p. 2480, 2019.
- [4] M. Arias, M. A. Campo-Bescos, and J. Alvarez-Mozos, "Crop classification based on temporal signatures of Sentinel-1 observations over Navarre province, Spain," *Remote Sens.*, vol. 12, no. 2, p. 278, 2020.
- [5] P. A. Rosen *et al.*, "Synthetic aperture radar interferometry," *Proc. IEEE*, vol. 88, no. 3, pp. 333–382, Mar. 2000.
- [6] T. Strozzi *et al.*, "Landuse mapping with ERS SAR interferometry," *IEEE Trans. Geosci. Remote Sens.*, vol. 38, no. 2, pp. 766–775, Mar. 2000.
- [7] M. Engdahl and J. Hyyppä, "Land-cover classification using multitemporal ERS-1/2 InSAR data," *IEEE Trans. Geosci. Remote Sens.*, vol. 41, no. 7, pp. 1620–1628, Jul. 2003.

- [8] F. Sica, A. Pulella, M. Nannini, M. Pinheiro, and P. Rizzoli, "Repeat-pass SAR interferometry for land cover classification: A methodology using Sentinel-1 short-time-series," *Remote Sens. Environ.*, vol. 232, 2019, Art. no. 111277.
- [9] A. W. Jacob *et al.*, "Sentinel-1 InSAR coherence for land cover mapping: A comparison of multiple feature-based classifiers," *IEEE J. Sel. Topics Appl. Earth Observ. Remote Sens.*, vol. 13, pp. 535–552, Jan. 2020.
- [10] M. Engdahl, M. Borgeaud, and M. Rast, "The use of ERS-1/2 Tandem interferometric coherence in the estimation of agricultural crop heights," *IEEE Trans. Geosci. Remote Sens.*, vol. 39, no. 8, pp. 1799–1806, Aug. 2001.
- [11] M. Busquier, J. M. Lopez-Sanchez, A. Mestre-Quereda, E. Navarro, M. P. Gonzalez-Dugo, and L. Mateos, "Exploring TanDEM-X interferometric products for crop-type mapping," *Remote Sens.*, vol. 12, no. 11, p. 1774, Jun. 2020.
- [12] R. Touzi, A. Lopes, J. Bruniquel, and P. W. Vachon, "Coherence estimation for SAR imagery," *IEEE Trans. Geosci. Remote Sens.*, vol. 37, no. 1, pp. 135–149, Jan. 1999.
- [13] L. Breiman, "Random forests," *Mach. Learn.*, vol. 45, pp. 5–32, 2001.
- [14] S. V. Stehman, "Selecting and interpreting measures of thematic classification accuracy," *Remote Sens. Environ.*, vol. 62, no. 1, pp. 77–89, Oct. 1997.
- [15] H. A. Zebker and J. Villasenor, "Decorrelation in interferometric radar echoes," *IEEE Trans. Geosci. Remote Sens.*, vol. 30, no. 5, pp. 950–959, Sep. 1992.
- [16] A. Veloso *et al.*, "Understanding the temporal behavior of crops using Sentinel-1 and Sentinel-2-like data for agricultural applications," *Remote Sens. Environ.*, vol. 199, pp. 415–426, 2017.
- [17] M. Vreugdenhil *et al.*, "Sensitivity of Sentinel-1 backscatter to vegetation dynamics: An Austrian case study," *Remote Sens.*, vol. 10, no. 9, p. 1396, 2018.
- [18] S. Khabbazan *et al.*, "Crop monitoring using Sentinel-1 data: A case study from The Netherlands," *Remote Sens.*, vol. 11, no. 16, p. 1887, 2019.
- [19] G. M. Foody, M. B. McCulloch, and W. B. Yates, "Crop classification from C-band polarimetric radar data," *Int. J. Remote Sens.*, vol. 15, no. 14, pp. 2871–2885, 1994.
- [20] J.-S. Lee, M. R. Grunes, and E. Pottier, "Quantitative comparison of classification capability: Fully polarimetric versus dual and single-polarization SAR," *IEEE Trans. Geosci. Remote Sens.*, vol. 39, no. 11, pp. 2343–2351, Nov. 2001.
- [21] D. H. Hoekman and M. A. M. Vissers, "A new polarimetric classification approach evaluated for agricultural crops," *IEEE Trans. Geosci. Remote Sens.*, vol. 41, no. 12, pp. 2881–2889, Dec. 2003.
- [22] H. McNairn, C. Champagne, J. Shang, D. Holmstrom, and G. Reichert, "Integration of optical and synthetic aperture radar (SAR) imagery for delivering operational annual crop inventories," *ISPRS J. Photogrammetry Remote Sens.*, vol. 64, no. 5, pp. 434–449, 2009.
- [23] H. Skriver, "Crop classification by multitemporal C- and L-band single- and dual-polarization and fully polarimetric SAR," *IEEE Trans. Geosci. Remote Sens.*, vol. 50, no. 6, pp. 2138–2149, Jun. 2012.
- [24] C. A. Deledalle, L. Denis, F. Tupin, A. Reigber, and M. Jager, "NL-SAR: A unified nonlocal framework for resolution-preserving (Pol)(In)SAR denoising," *IEEE Trans. Geosci. Remote Sens.*, vol. 53, no. 4, pp. 2021–2038, Apr. 2015.



Alejandro Mestre-Quereda (Member) was born in Madrid, Spain, in 1990. He received the B.S. degree in telecommunication engineering, in 2015, the M.Sc. degree in telecommunication engineering, in 2017, and the Ph.D. degree, in 2019, from the University of Alicante (UA), Spain.

Currently, he is a Postdoctoral Researcher with the Signals, Systems and Telecommunication (SST) group, University of Alicante, Spain. His research interests include the development of advanced signal processing techniques for SAR interferometry and polarimetry, and the exploitation of SAR/InSAR data for new applications including land-cover and vegetation mapping.



Juan M. Lopez-Sanchez (Senior Member, IEEE) was born in Alicante, Spain, in 1972. He received the Ingeniero (M.S.) and Doctor Ingeniero (Ph.D.) degrees in telecommunication engineering from the Technical University of Valencia (UPV), Valencia, Spain, in 1996 and 2000, respectively.

From 1998 to 1999, he worked as a Predoctoral Grantholder with the Space Applications Institute, Joint Research Centre of the European Commission, Ispra, Italy. Since 2000, he leads the Signals, Systems and Telecommunication Group of the University of Alicante, Spain, where he is a Full Professor since November 2011. His research interests include microwave remote sensing for inversion of biophysical parameters, polarimetric and interferometric techniques, SAR imaging algorithms, and applications of radar remote sensing in agriculture and geophysics. He has coauthored more than 80 papers in refereed journals and more than 130 papers and presentations in international conferences and symposia.

Dr. Lopez-Sanchez received the Indra Award for the best Ph.D. thesis about radar in Spain, in 2001. From 2006 to 2012, he was the Chair of the Spanish Chapter of the IEEE Geoscience and Remote Sensing Society.



Fernando Vicente-Guijalba (Member) was born in Alicante, Spain, in 1981. He received the B.Sc. and M.Sc. degrees in telecommunications engineering and the Ph.D. degree in computer science from the University of Alicante, Alicante, Spain, in 2011, 2014, and 2016, respectively.

From 2011 to 2016, he was a Junior Researcher with the Signals, Systems and Telecommunications (SST) Group, University of Alicante. Since 2017, he has been part of Dares Technology, Barcelona, Spain, and since 2019, he has been leading the institutional projects division of the company. His research interests include the application of multispectral and radar data for land cover and vegetation mapping.



Alexander W. Jacob (Member) holds a licentiate degree in geoinformatics from KTH Royal Institute of Technology, Sweden.

He coordinates the research group Advanced Computing for Earth Observation, Institute for Earth Observation with the objective to foster EO data science. He is an experienced researcher and software developer in the field of Earth Observation (5+ years of experience). He is responsible for the scientific data management including the organization of multidimensional raster data and coordination of algorithm development in operational and research processing chains. He is currently an active Project Manager for Eurac Research's contribution to the H2020 openEO project and the ESA SEOM SInCohMap project as well as several internal development projects.



Marcus E. Engdahl received the M.Sc. degree in technology (technical physics) from the Helsinki University of Technology, in 1996, and the D.Sc. degree in technology (electrical engineering) from Aalto University, Helsinki, Finland, in 2013. In 1999, he completed the Summer Session Course, Nakhon Ratchasima, Thailand, organized by the International Space University (Strasbourg, France).

He has been an Earth Observation Applications Engineer with ESA-ESRIN, Frascati, Italy since August 2003. In ESA, he has been involved with algorithm development and scientific data utilization of ERS-1/2, Envisat, Sentinel-1, and CryoSat-2 missions. He is actively involved with the evolution of the Sentinel-1 mission and preparation for the BIOMASS mission. He is responsible for the ESA SNAP toolbox development, including Sentinel-1 Toolbox and its predecessor ESA NEST toolbox. His research interests include biogeophysical parameter retrieval from multitemporal InSAR data, scientific utilization of SAR and InSAR data, algorithm and software development, remote sensing of the cryosphere, glaciology, and monitoring of the polar ice sheets from space.